

**International Journal of Power Electronics**

ISSN online: 1756-6398 - ISSN print: 1756-638X  
<https://www.inderscience.com/ijpelec>

---

**Controller optimisation under different drive cycles for induction motor driven electric vehicle fed through multilevel inverter**

Paramjeet Singh Jamwal, Sanjeev Singh, Shailendra Jain

**DOI:** [10.1504/IJPELEC.2024.10054731](https://doi.org/10.1504/IJPELEC.2024.10054731)

**Article History:**

Received:	06 August 2022
Last revised:	07 November 2022
Accepted:	22 January 2023
Published online:	23 December 2023

---

# Controller optimisation under different drive cycles for induction motor driven electric vehicle fed through multilevel inverter

---

Paramjeet Singh Jamwal\*

Department of Electrical and Instrumentation Engineering,  
Sant Longowal Institute of Engineering and Technology,  
Longowal, Sangrur, Punjab, India

Email: paramjeet\_pei1803@sliet.ac.in

\*Corresponding author

Sanjeev Singh

Department of Electrical Engineering,  
Maulana Azad National Institute of Technology,  
Bhopal, Madhya Pradesh, India

Email: sschauhan@manit.ac.in

Shailendra Jain

Department of Electrical and Instrumentation Engineering,  
Sant Longowal Institute of Engineering and Technology,  
Longowal, Sangrur, Punjab, India

Email: director@sliet.ac.in

**Abstract:** Vector controlled induction motors (IMs) are used in electric vehicles (EVs) for effective speed control. The use of three-level inverter (3LI) offers the advantage of reduced switch stress along with lower total harmonic distortion in voltage (THD<sub>v</sub>) over two-level inverters. An indirect current vector control (ICVC) scheme has one proportional-integral (PI) controller for speed control of EV. The selection of controller coefficients affects the performance of complete drive. Therefore, this paper uses particle swarm optimisation technique for optimum selection of controller coefficients used for the control of CHB3LI fed IM drive. This drive is tested under CBD, COMMUTER, and EU driving cycles on three torque loadings through simulation in MATLAB Simulink and validated experimentally on a reduced scale laboratory setup. The obtained results are presented to demonstrate desired performance under all the driving cycles for optimised controller coefficients along with improved THD<sub>v</sub> and reduced losses in the IM.

**Keywords:** cascaded H-bridge; CHB; controller optimisation; driving cycle; electric vehicle; indirect current vector control; ICVC; induction motor drive; particle swarm optimisation; PSO; proportional-integral controller; three-level inverter; 3LI.

**Reference** to this paper should be made as follows: Jamwal, P.S., Singh, S. and Jain, S. (2024) 'Controller optimisation under different drive cycles for induction motor driven electric vehicle fed through multilevel inverter', *Int. J. Power Electronics*, Vol. 19, No. 1, pp.53–78.

**Biographical notes:** Paramjeet Singh Jamwal completed his BTech in Electrical and Electronics Engineering from the College of Engineering Roorkee (COER), Roorkee, Uttarakhand, India, in 2011, and MTech in Instrumentation and Control Engineering from the Sant Longowal Institute of Engineering and Technology (SLIET), Longowal, Punjab, India, in 2015. Presently, he is working towards his PhD at the SLIET Longowal since 2018. He was a Lecturer from 2011–2013 with Guru Nanak Education Trust Group of Institutions, Roorkee, an Assistant Professor in 2016 with PHONICS Group of Institutions, Roorkee, and an Assistant Professor in 2017 with Roorkee College of Engineering (RCE), Roorkee, Uttarakhand, India. He has contributed more than seven research articles. His research interests include multilevel inverters, induction motor drive, particle swarm optimisation, and permanent magnet synchronous motor drive.

Sanjeev Singh received his BE in Electrical Engineering from the Government Engineering College (GEC), Rewa, Madhya Pradesh, India, in 1993, MTech in Energy Management from the Devi Ahilya Vishwavidyalaya (DAVV), Indore, Madhya Pradesh, India, in 1997 and PhD from the Indian Institute of Technology (IIT), Delhi, New Delhi, India, in 2010. He was a Postdoctoral Research Fellow at the École de Technologie Supérieure, Montréal, QC, Canada, in 2016–2017. He was an Assistant Professor from 2000–2013 and an Associate Professor from 2013–2019 with SLIET Longowal. Presently, he is a Professor in the Electrical Engineering Department of Maulana Azad National Institute of Technology (MANIT), Bhopal, Madhya Pradesh, India. He has contributed 2 books and more than 90 research articles. His research interests include power electronics and drives, power quality, electric vehicles, microgrids, and grid integration of renewable energy generators.

Shailendra Jain received his BE in Electrical Engineering from the Samrat Ashok Technological Institute (SATI), Vidisha, Madhya Pradesh, India, in 1990, ME in Power Electronics from the Shri Govindram Seksaria Institute of Technology and Science (SGSITS), Indore, Madhya Pradesh, India, in 1994, and PhD from the Indian Institute of Technology (IIT), Roorkee, Uttarakhand, India, in 2003. He was a Postdoctoral Research Fellow at the University of Western Ontario, London, ON, Canada, in 2007. Presently, he is the Director of SLIET Longowal since 2017 and on deputation from MANIT Bhopal, where he is a Professor in the Department of Electrical Engineering. He has contributed two books and more than 100 research articles. His research interests include power electronics and electric drives, power quality improvement, active power filters, high-power-factor converters, and fuel-cell-based distributed generation.

---

## 1 Introduction

Squirrel cage induction motor (IM) is being used in electric vehicles (EVs), as a low cost and maintenance free option in comparison to brushless permanent magnet (PM) motors (Kousalya et al., 2022). Precise speed control is the only specific requirement of IM, which is achieved through vector controlled two-level inverters (2LIs) in present EVs. The 2LIs result higher switch stress and high total harmonic distortion (THD) in voltage waveform. Both these aspects result in increased losses and reduced system reliability (Mishra and Maheshwari, 2020). Multilevel inverters (MLIs) offer dual advantage in terms of reduced switch stress and reduced total harmonic distortion in output voltage (THDv) (Poorfakhraei et al., 2021). A cascaded H-bridge (CHB) inverter offer modular

configuration with minimum switch count for three-phase supply. Single-phase reduced device count (RDC) cascaded H-bridge seven-level inverter (CHB7LI) is reported by Armi et al. (2020). The discussion is made about inverter output voltage and harmonic spectrum but no discussion is made about loading of inverter. Three-phase CHB7LI along with several optimisation techniques is reported in Kundu et al. (2020). A cascaded H-bridge three-level inverter (CHB3LI) results in lower THDv and lesser switch stress as compared to 2LI of similar rating (Jamwal et al., 2022).

EV application faces sudden change in the speed, which is to be managed in the inverter fed IM drive (IMD). This speed change varies with change in driving cycle. Several driving cycles is reported by Xu et al. (2022). The performance of IMD is tested with New York City cycle (NYCC) and new European driving cycle (NEDC) by Prabhakar et al. (2018). The performance of indirect current vector control (ICVC) scheme fed IMD depends upon the proportional-integral (PI) speed controller (Krishnan, 2015). The selection of global best proportional and integral gains ( $K_{GBPS}$  and  $K_{GBIS}$ ) of PI speed controller, is a challenging task under different loading and driving cycle (Hannana et al., 2018). To face this challenge, particle swarm optimisation (PSO) technique is used in this work because of its fast convergence and easy implementation (Kennedy and Eberhart, 1995).

The initialisation of particles in the PSO technique is an important and foremost step. Most of the researchers are using random approach to initialise the particles (Singh and Singh, 2014). With the random approach, particles are not uniformly distributed in the complete search space, so PSO technique may take longer time to find the optimum value. Therefore, square particle generation approach is reported by Jamwal and Singh (2016) to initialise the particles in the complete search space. Square particle generation approach divides the complete search space in to a small search space for each particle and uniformly distributes the particles in the complete search space. The selection of the inertia weight decides the exploration and convergence behaviour of PSO technique, which varies with the application (Bansal et al., 2011). The exploration and convergence behaviour of PSO technique can also be controlled by varying the acceleration constant. Recently, PSO technique is reported to optimise the controller of static synchronous series compensator (Rohit et al., 2022), maximum power point tracking in solar photovoltaic system (Nagadurga et al., 2021), optimise the finite state model predictive controller (Lammouchi and Barra, 2020) and optimum utilisation of hybrid renewable energy system (Suresh et al., 2020).

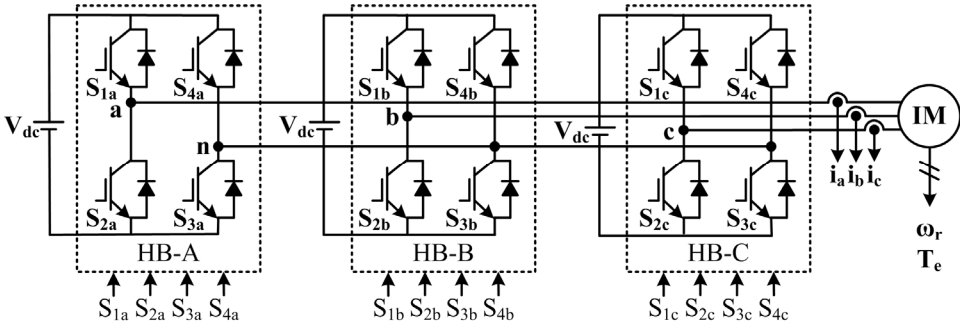
In this work, variable acceleration constant is taken to utilise the exploration and convergence behaviour of PSO technique to optimise the PI speed controller of ICVC scheme. The PI speed controller is optimised for central business district (CBD), COMMUTER, and extra urban (EU) driving cycles separately with three torque loadings. This paper is presented in four sections. The need and importance of optimisation techniques for IMD application is already discussed in Section 1. A CHB3LI fed IM, ICVC scheme, output voltage with THDv spectrum of inverters, driving cycles, EV loading calculation, and PSO technique are described in Section 2. The optimised coefficients of PI speed controller, simulation results with different driving cycles, and experimental results are described in Section 3. The conclusion from the work is discussed in Section 4.

## 2 IM drive

### 2.1 CHB3LI fed IM

Three-phase IM is operated with three-phase supply generated with CHB3LI. This CHB3LI consists of three single-phase H-bridge inverters, as shown in Figure 1. Each H-bridge is designed with two legs and powered with separate dc source ( $V_{dc}$ ). Each leg consists of two IGBT switch in series. First leg of each H-bridge generates three-phases (a, b, c) of three-phase supply and fed to three-phase IM. Second leg of each H-bridge generates neutral which are shorted. Twelve switching signals ( $S_{1a-4a}$ ,  $S_{1b-4b}$ , and  $S_{1c-4c}$ ) are required to operate the three H-bridges (HB-A, HB-B, and HB-C). These switching signals are generated with ICVC scheme. The brief description about ICVC scheme is given in next section. This ICVC scheme operates on the basis of sensed three-phase currents ( $i_a$ ,  $i_b$ , and  $i_c$ ) and rotor speed ( $\omega_r$ ).

**Figure 1** Schematic diagram of CHB3LI fed IM



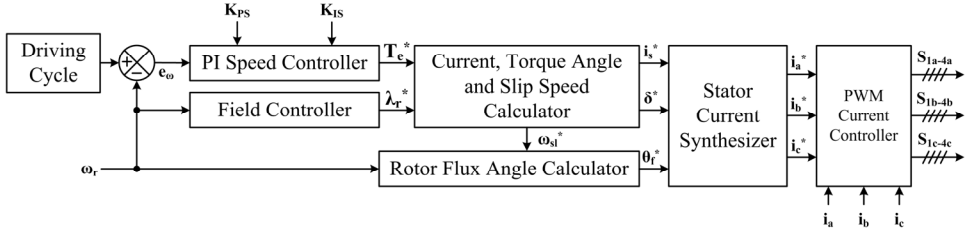
### 2.2 ICVC scheme

A control scheme, in which field and torque components of current is controlled separately, is known as vector control (Krishnan, 2015). A vector control scheme, in which, these field and torque components of current is estimated from speed only, is known as indirect vector control. An indirect vector control scheme, in which three-phase stator current reference ( $i_a^*$ ,  $i_b^*$ , and  $i_c^*$ ) along with three-phase sensed stator current ( $i_a$ ,  $i_b$ , and  $i_c$ ), is used to generates switching signals, is known as ICVC (Jamwal et al., 2022). The schematic diagram of an ICVC scheme is given in Figure 2.

Firstly, rotor speed ( $\omega_r$ ) is compared with selected driving cycle (see Subsection 2.4) to obtain speed error ( $e_\omega$ ). This speed error is fed to PI speed controller to obtain necessary electromagnetic torque reference ( $T_e^*$ ). Rotor speed is also fed to field controller to obtain rotor flux linkage reference ( $\lambda_r^*$ ). This electromagnetic torque reference and rotor flux linkage reference is used to obtain stator current reference ( $i_s^*$ ), torque angle reference ( $\delta^*$ ), and slip speed reference ( $\omega_{sl}^*$ ). Slip speed reference, along with rotor speed, is used to obtain field angle reference ( $\theta_f^*$ ). Stator current reference, torque angle reference, and field angle reference is fed to stator current synthesiser to obtain three-phase stator current reference ( $i_a^*$ ,  $i_b^*$ , and  $i_c^*$ ). This reference and sensed

three-phase stator current ( $i_a$ ,  $i_b$ , and  $i_c$ ) is fed to pulse width modulation (PWM) current controller to obtain switching signals ( $S_{1a-4a}$ ,  $S_{1b-4b}$ , and  $S_{1c-4c}$ ).

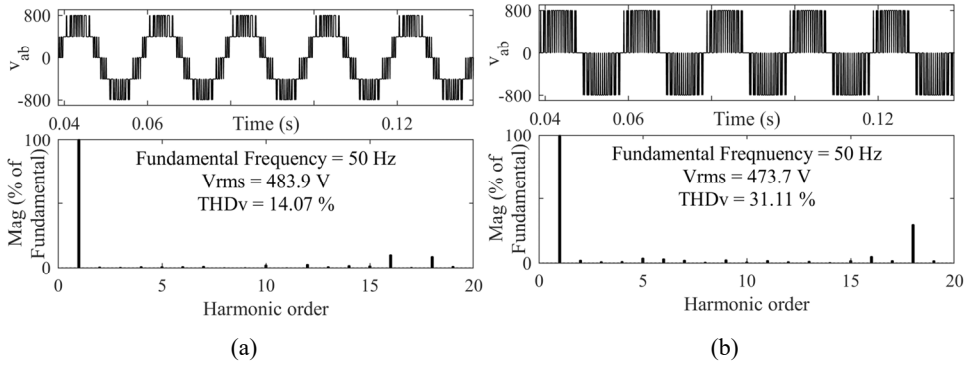
**Figure 2** Schematic diagram of ICVC scheme



### 2.3 Output line-voltage and THDv

Output line-voltage ( $V_{ab}$ ) along with THDv spectrum of CHB3LI is shown in Figure 3(a). It shows that, standing voltage for a switch of CHB3LI is 400 V while THDv is 14.07%. Output line-voltage ( $V_{ab}$ ) along with THDv spectrum of 2LI is given in Figure 3(b). It shows that standing voltage for a switch of 2LI is 800 V while THDv is 31.11%.

**Figure 3** Output line-voltage and THDv of inverters, (a) CHB3LI (b) 2LI



The RMS voltage for both the inverters is between (473.7 to 483.9 V). Therefore, it is obvious that, with the use of CHB3LI in place of conventional 2LI, there is 50% reduction in standing voltage for a switch and 54.5% reduction in THDv.

### 2.4 Driving cycles

A cycle, which includes start, acceleration, cruise, deceleration, and/or stop mode, is known as driving cycle. There are various driving cycles reported by Xu et al. (2022). In this work, three driving cycles named as CBD, COMMUTER, and EU are considered to test the performance of CHB3LI fed IMD.

2.4.1 CBD driving cycle

There are three operating modes (acceleration, cruise, and deceleration), two standby modes (start, and stop) and two speed levels ( $\omega_0$  and  $\omega_{15}$ ) in CBD driving cycle (Figure 4). Acceleration, cruise, and deceleration mode are represented with  $\delta_1$ ,  $\delta_2$ , and  $\delta_3$  respectively. Start and stop mode is represented with  $\delta_0$  and  $\delta_4$ . The time duration of driving cycle is calculated with equation (1).

$$t_{dc} = s_{dc} \times n_{dc} \tag{1}$$

where  $t_{dc}$ ,  $s_{dc}$ , and  $n_{dc}$  are time duration, size of section, and number of sections of driving cycle.

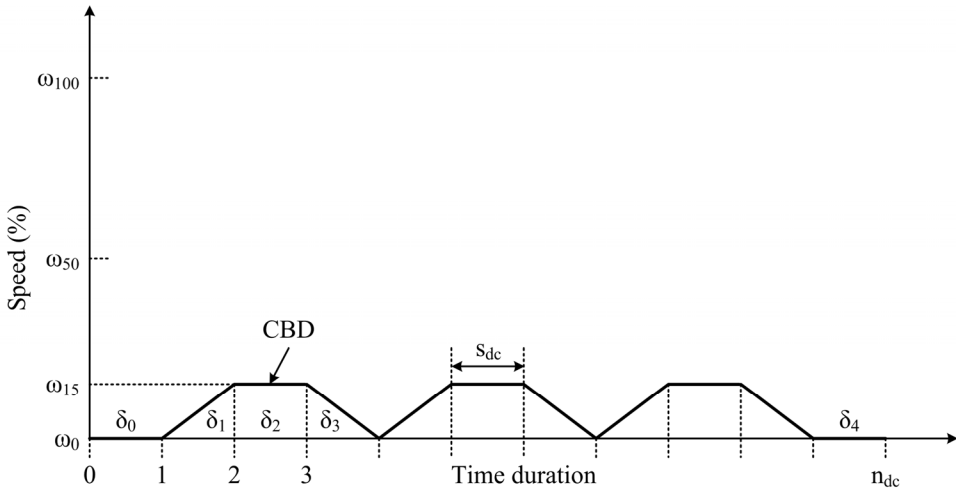
2.4.2 COMMUTER driving cycle

There are three operating modes (acceleration, cruise, and deceleration), two standby modes (start and stop) and two speed levels ( $\omega_0$  and  $\omega_{45}$ ) in COMMUTER driving cycle (Figure 5). Acceleration, cruise, and deceleration mode are represented with  $\delta_1$ ,  $\delta_2$ , and  $\delta_3$  respectively. Start and stop mode is represented with  $\delta_0$  and  $\delta_4$ .

2.4.3 EU driving cycle

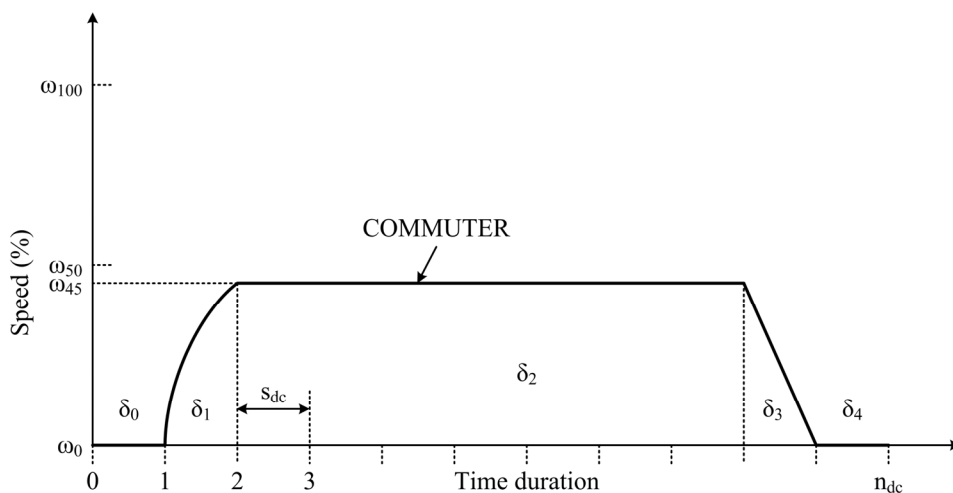
There are three operating modes (acceleration, cruise, and deceleration), two standby modes (start and stop) and five speed levels ( $\omega_0$ ,  $\omega_{40}$ ,  $\omega_{50}$ ,  $\omega_{85}$ , and  $\omega_{100}$ ) in EU driving cycle as shown in Figure 6.

Figure 4 CBD driving cycle



Acceleration, cruise, and deceleration mode is represented with ( $\delta_1$ ,  $\delta_6$ ,  $\delta_8$ , and  $\delta_{10}$ ), ( $\delta_2$ ,  $\delta_5$ ,  $\delta_7$ ,  $\delta_9$ , and  $\delta_{11}$ ), and ( $\delta_3$ , and  $\delta_{12}$ ), respectively. Start and stop mode is represented with  $\delta_0$  and  $\delta_4$ . Operating and standby mode of these driving cycles are listed in Table 1.

**Figure 5** COMMUTER driving cycle



**Figure 6** EU driving cycle

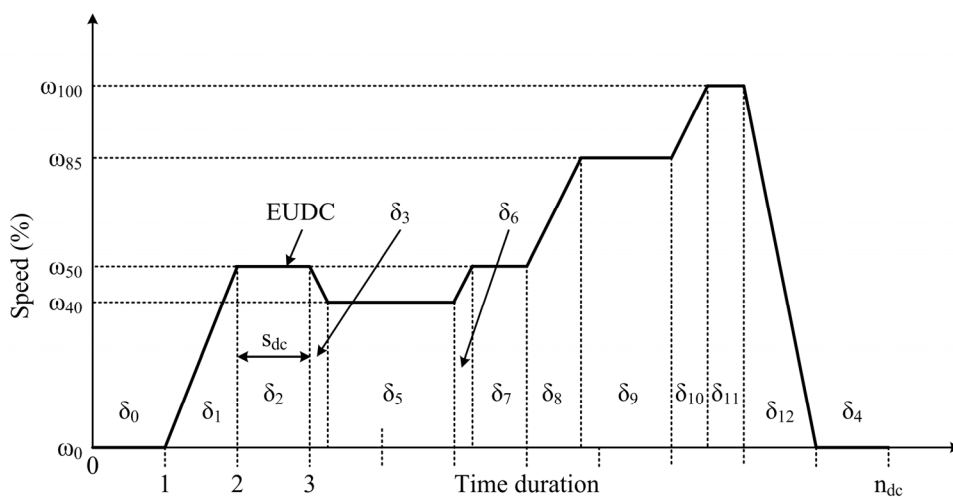


**Table 1** Operating and standby mode of driving cycles

Mode	Driving cycle		
	CBD	COMMUTER	EU
Start	$\delta_0$	$\delta_0$	$\delta_0$
Acceleration	$\delta_1$	$\delta_1$	$\delta_1, \delta_6, \delta_8, \delta_{10}$
Cruise	$\delta_2$	$\delta_2$	$\delta_2, \delta_5, \delta_7, \delta_9, \delta_{11}$
Deceleration	$\delta_3$	$\delta_3$	$\delta_3, \delta_{12}$
Stop	$\delta_4$	$\delta_4$	$\delta_4$

### 2.5 Percentage loading calculation for EV

The weight of an EV is measured in two ways, i.e., without passengers and with passengers. When an EV is weighted without passengers, the weight is known as unladen kerb weight. When an EV is weighted with passengers, the weight is known as gross weight. Both these weights are fixed for every EV before manufacturing. In this work, Mahindra Electric e2o Plus (n.d.) is considered for percentage loading calculation because it uses a three-phase IM as a traction motor. Mahindra Electric e2o Plus has 937 kg unladen kerb weight, 1,257 kg gross weight, and five passenger seating capacity including driver. From this data, the weight of a passenger ( $W_P$ ) is calculated.

The  $W_P$  is:

$$W_P = \frac{W_G - W_K}{N} \quad (2)$$

where  $W_G$  is the gross weight of the EV,  $W_K$  is the Kerb weight of the EV, and  $N$  is the number of passengers.

The percentage loading of the EV with  $N$  passengers is:

$$\text{Percentage loading} = \frac{(W_K + W_P \times N)}{W_G} \times 100 \quad (3)$$

The calculated and considered percentage loading of the EV from equations (2) and (3) with different passengers is given in Table 2. This percentage loading is used to select the percentage torque for IMD.

**Table 2** Calculation of percentage loading of EV

<i>Number of passengers</i>	<i>Calculated percentage loading</i>	<i>Considered percentage loading</i>
1	79.63	80
2	84.73	85
3	89.82	90
4	94.91	95
5	100.0	100

### 2.6 PSO technique

An optimisation technique, which generates swarm of particles, is known as PSO. The schematic diagram of PSO technique is shown in Figure 7. PSO technique needs some parameters to initialise the proportional and integral coefficients of PI speed controller ( $K_{PS}$  and  $K_{IS}$ ) for each particle. These parameters are number of particles ( $N_P$ ), number of iteration ( $N_i$ ), minimum proportional gain ( $K_{PSmin}$ ), maximum proportional gain ( $K_{PSmax}$ ), minimum integral gain ( $K_{ISmin}$ ), and maximum integral gain ( $K_{ISmax}$ ). PSO technique need a fitness function to test and update the present proportional and integral value of PI speed controller for next iteration. This fitness function needs the value of speed error ( $e_\omega$ ) and torque error ( $e_T$ ).

Figure 7 Schematic diagram of PSO technique

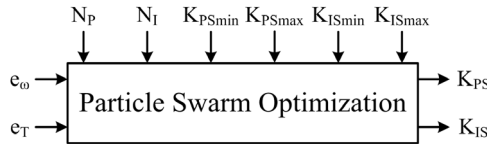
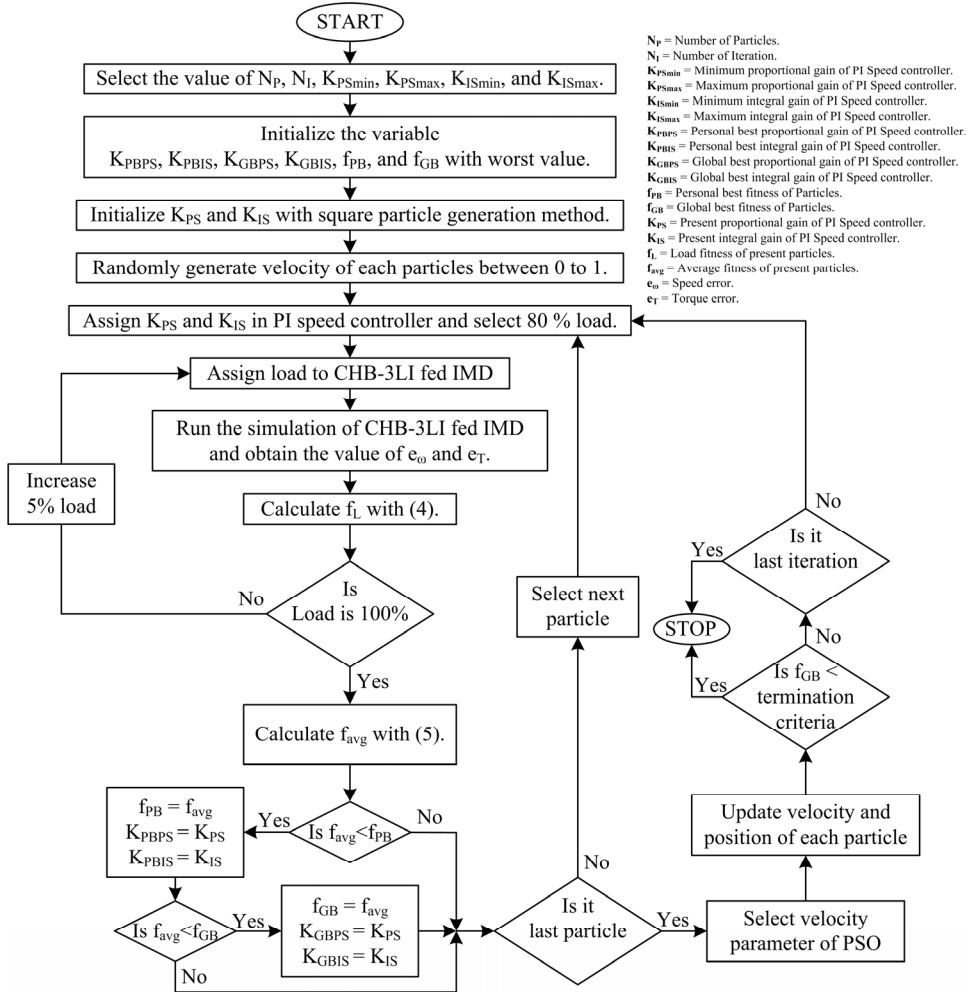


Figure 8 Flowchart of PSO technique



The flowchart of the PSO technique is shown in Figure 8. This PSO technique includes following steps:

- 1 Obtain the value of number of particles ( $N_p$ ), number of iteration ( $N_i$ ), minimum proportional gain ( $K_{psmin}$ ), maximum proportional gain ( $K_{psmax}$ ), minimum integral gain ( $K_{ismin}$ ), and maximum integral gain ( $K_{ismax}$ ).

- 2 Initialise the value of personal best proportional gain ( $K_{PBPS}$ ), personal best integral gain ( $K_{PBIS}$ ), global best proportional gain ( $K_{GBPS}$ ), global best integral gain ( $K_{GBIS}$ ), personal best fitness ( $f_{PB}$ ), and global best fitness ( $f_{GB}$ ) with worst value.
- 3 Initialise the present proportional and integral gain ( $K_{PS}$  and  $K_{IS}$ ) value for each particle with square particle generation method (Jamwal and Singh, 2016).
- 4 Randomly generate the velocity of each particle in the range of 0 to 1.
- 5 Assign the present proportional and integral gain ( $K_{PS}$  and  $K_{IS}$ ) value of a particle to PI speed controller and select minimum load (80%) equivalent to only driver in the EV (Table 2).
- 6 Assign load to CHB3LI fed IMD.
- 7 Run the simulation of CHB3LI fed IMD and obtain the value of speed error ( $e_{\omega}$ ) and torque error ( $e_T$ ).
- 8 Calculate the load fitness ( $f_L$ ) of CHB3LI fed IMD with equation (4). There are two objectives achieved through this objective function. First one is optimum speed error ( $e_{\omega}$ ) and second one is optimum torque error ( $e_T$ ). The optimum speed and torque errors ( $e_{\omega}$  and  $e_T$ ) for CBD, COMMUTER, and EU driving cycles are listed in Table 3.

$$f_L = w_{\omega f} \times e_{\omega} + w_{Tf} \times e_T \quad (4)$$

where  $w_{\omega f}$  and  $w_{Tf}$  are speed fitness weightage and torque fitness weightage.

- 9 Check the load, if it is 100% then jump to step 11 otherwise go to next step 10.
- 10 Increase the load by 5% and go back to step 6.
- 11 Calculate the average fitness ( $f_{avg}$ ) of CHB3LI fed IMD with equation (5). For this, first, load fitness ( $f_L$ ) is calculated on all five-loads listed in Table 2. The value of  $n$  is considered between 16 to 20 to represent load on EV for single to five passengers, respectively. For example, when the value of  $n$  is 16, the loading comes as 80% which is for only driver sitting in the EV, thereafter, 17, 18, 19 and 20 shall give loadings percentage of 85, 90, 95 and 100, respectively, as per Table 2. In this way, the fitness of gain parameters of PI speed controller is obtained on all five-loads. The average fitness ( $f_{avg}$ ) for CBD, COMMUTER, and EU driving cycles are listed in Table 3.

$$f_{avg} = \frac{1}{5} \sum_{n=16}^{n=20} f_L(5 \times n) \quad (5)$$

- 12 Compare the average fitness with personal best fitness ( $f_{PB}$ ) of CHB3LI fed IMD, if average fitness is lesser than personal best fitness then updates the value of  $f_{PB}$  with  $f_{avg}$ ,  $K_{PBPS}$  with  $K_{PS}$ , and  $K_{PBIS}$  with  $K_{IS}$  and go to next step 13. Otherwise jump to step 14.
- 13 Compare the average fitness with global best fitness ( $f_{GB}$ ) of CHB3LI fed IMD, if average fitness is lesser than global best fitness then updates the value of  $f_{GB}$  with  $f_{avg}$ ,  $K_{GBPS}$  with  $K_{PS}$ , and  $K_{GBIS}$  with  $K_{IS}$  and go to next step 14. Otherwise directly go to next step 14.

- 14 Check the particle number, if it is the last particle of the swarm then go to next step 15 otherwise select next particle and go back to step 5.
- 15 Update velocity and gain parameters ( $K_{PS}$  and  $K_{IS}$ ) for each particle of the swarm (Kennedy and Eberhart, 1995; Bansal et al., 2011) with equations (6)–(7) and (8)–(9), respectively.

$$v(k+1) = w_i \times v(k) + c_1 \times r_1 (K_{PBPS} - K_{PS}) + c_2 \times r_2 (K_{GBPS} - K_{PS}) \quad (6)$$

$$v(k+1) = w_i \times v(k) + c_1 \times r_1 (K_{PBIS} - K_{IS}) + c_2 \times r_2 (K_{GBIS} - K_{IS}) \quad (7)$$

$$K_{PS}(k+1) = K_{PS} + v(k+1) \quad (8)$$

$$K_{IS}(k+1) = K_{IS} + v(k+1) \quad (9)$$

where  $r_1$  and  $r_2$  are random parameter varying between 0 to 1, while  $c_1$  and  $c_2$  are acceleration constant taken as 1.49618 and 0.74809 for iterations 1–10 and 11–20, respectively.

- 16 Check termination criteria, if  $f_{GB}$  is lesser than termination criteria then stop the PSO technique otherwise go to next step 17.
- 17 Check the iteration number, if it is the last iteration then stop the PSO technique otherwise go back to step 5.

With PSO technique, global best value of proportional and integral coefficients of PI speed controller is obtained for all three driving cycles and given in Table 3.

### 3 Results and discussion

#### 3.1 Optimised coefficients of PI speed controller

For optimisation of PI controller coefficients, a swarm of 25 numbers of particles are selected for each driving cycle. Each particle has personal best proportional and integral gain value ( $K_{PBPS}$  and  $K_{PBIS}$ ). The personal best proportional and integral gain value for each particle with CBD driving cycle is given in Figure 9. After 1st iteration, particles are scattered in complete range (0–15) of proportional and integral gain value because of square particle generation method (Jamwal and Singh, 2016), as shown in Figure 9(a).

After 2nd iteration, particles gather between 3.49 to 4.55 and 1.76 to 2.76 for  $K_{PBPS}$  and  $K_{PBIS}$ , respectively, as shown in Figure 9(b). After 10th iteration, swarm of particles shift towards the right side and further narrow down their search range between 6.4 to 7.69 and 0.6 to 1.3 for  $K_{PBPS}$  and  $K_{PBIS}$ , respectively, as shown in Figure 9(c). After 20th iteration, swarm of particles further shift towards right side and further narrow down their search range between 7.32 to 7.83 and 0.61 to 0.84 for  $K_{PBPS}$  and  $K_{PBIS}$ , respectively, as shown in Figure 9d. The obtained value of global best proportional and integral gain ( $K_{GBPS}$  and  $K_{GBIS}$ ) with CBD driving cycle is 7.821584 and 0.691534.

The personal best proportional and integral gain value for each particle with COMMUTER driving cycle is given in Figure 10. After 1st iteration, particles are scattered in complete range (0–15) of proportional and integral gain value, as shown in Figure 10(a). After 2nd iteration, swarm of particles narrow down their search range

between 0 to 5.8 and 0 to 13 for  $K_{PBPS}$  and  $K_{PBIS}$ , respectively, as shown in Figure 10(b). After 10th iteration, particles further narrow down their search range between 4.6 to 6.2 and 0.41 to 0.99 for  $K_{PBPS}$  and  $K_{PBIS}$  and shift to the right side, respectively, as shown in Figure 10(c). After 20th iteration, particles further narrow down their search range between 5.64 to 5.93 and 0.62 to 0.73 for  $K_{PBPS}$  and  $K_{PBIS}$ , respectively, as shown in Figure 10(d). The obtained value of global best proportional and integral gain ( $K_{GBPS}$  and  $K_{GBIS}$ ) with COMMUTER driving cycle is 5.782789 and 0.715844.

**Figure 9** Personal best proportional and integral gain ( $K_{PBPS}$  and  $K_{PBIS}$ ) with CBD driving cycle, (a) after 1st iteration (b) after 2nd iteration (c) after 10th iteration (d) after 20th iteration

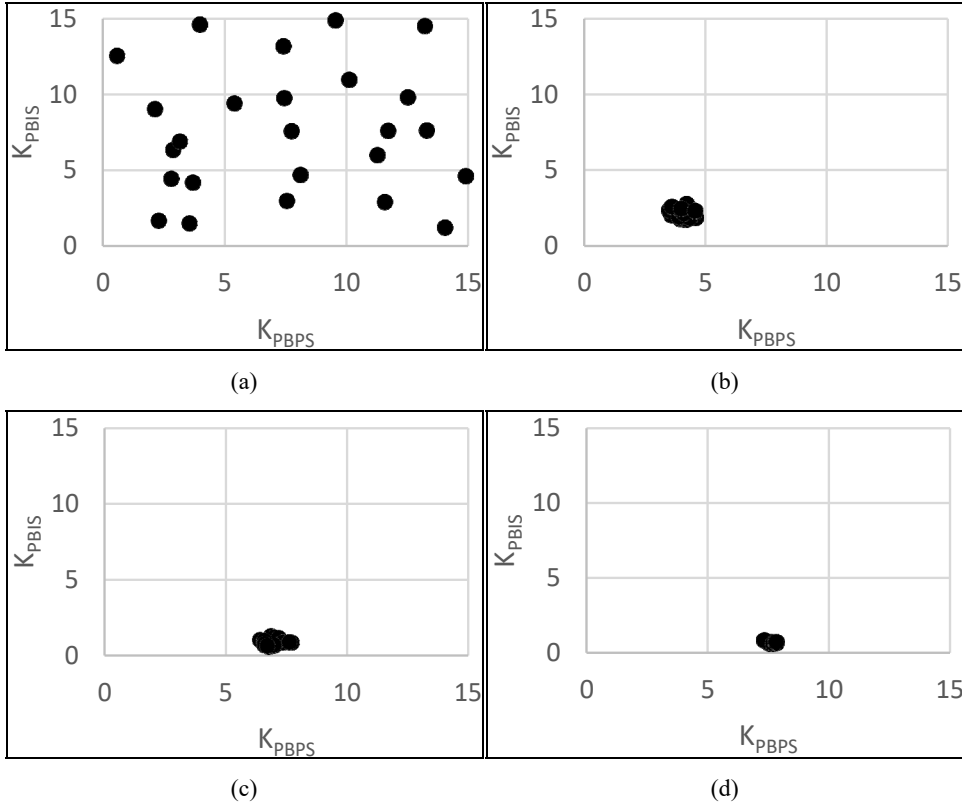
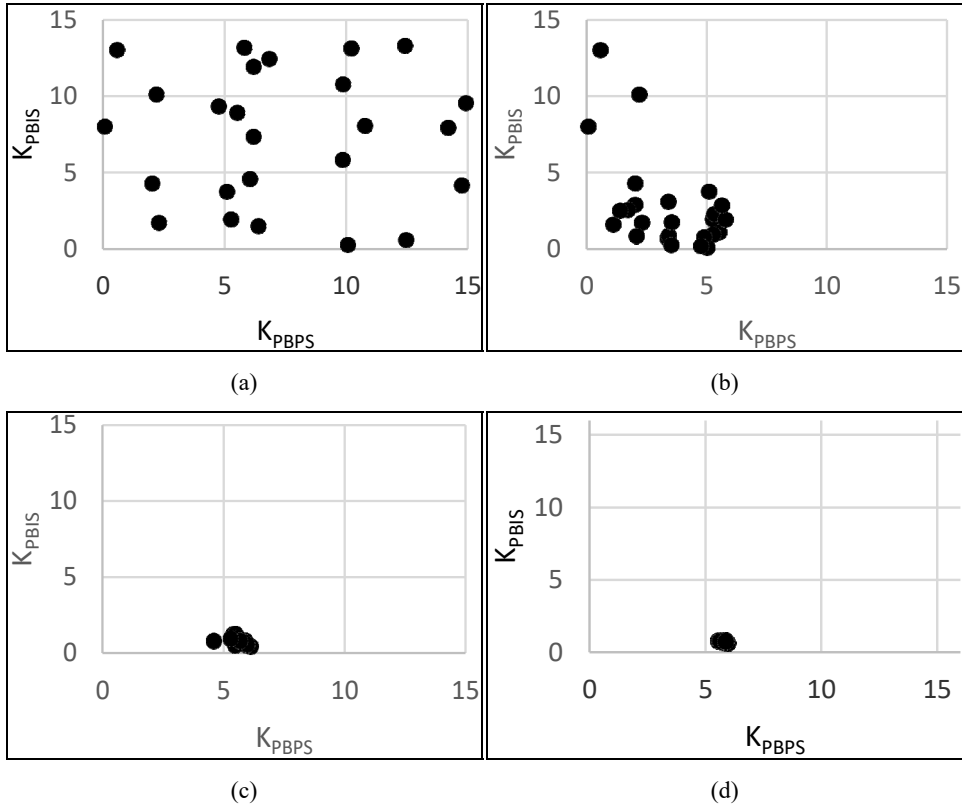


Figure 11 shows the personal best proportional and integral gain for each particle with EU driving cycle.

After 1st iteration, particles are scattered in complete range (0–15) of proportional and integral gain value, as shown in Figure 11(a). After 2nd iteration, particles narrow down their search range between 0 to 8 and 0 to 11, for  $K_{PBPS}$  and  $K_{PBIS}$  both, as shown in Figure 11(b). After 10th iteration, all particles gather at a point and further narrow down their search range between 3.7 to 4.5 and 8.9 to 9.8 for  $K_{PBPS}$  and  $K_{PBIS}$ , respectively, as shown in Figure 11(c). After 20th iteration, swarm of particles further narrow down their search range between 4.08 to 4.5 and 9.0 to 9.8 for  $K_{PBPS}$  and  $K_{PBIS}$ , respectively, as shown in Figure 11(d). The obtained value of global best proportional and integral gain ( $K_{GBPS}$  and  $K_{GBIS}$ ) with EU driving cycle is 4.328747 and 9.416067.

**Figure 10** Personal best proportional and integral gain ( $K_{PBPS}$  and  $K_{PBIS}$ ) with COMMUTER driving cycle, (a) after 1st iteration (b) after 2nd iteration (c) after 10th iteration (d) after 20th iteration



The obtained value of minimum speed error ( $e_w$ ), minimum torque error ( $e_T$ ), global best fitness ( $f_{GB}$ ), global best proportional gain ( $K_{GBPS}$ ), and global best integral gain ( $K_{GBIS}$ ) with CBD, COMMUTER, and EU driving cycle are listed in Table 3. The global best proportional and integral gain parameters dictate the value of speed controller coefficients in IM driven EVs fed through a MLI for three driving cycles. These values of global best proportional and integral gain, with different driving cycles, are used to analyse the performance of IMD.

The speed controller coefficients affect the motor drives performance in two ways. If the controller is tuned for optimum speed/torque error in complete drive cycle (as the presented case), it results in different speed/torque error during different parts of the drive cycle but, reduces errors during starting and other transients also.

On the other hand, if the controller is tuned separately for a particular loading/speed condition, it may result high errors during other speed/loading and transients. To handle such situation, different controller coefficients are required to obtain desired speed response at different speeds. This makes the algorithm complex and yields different values of controller coefficients for different operating conditions (such as starting, acceleration/retardation, cruise, etc.). The presented work has used the optimisation

objective of a cumulative speed and torque error in complete drive cycle and obtained good results for all the presented drive cycles.

**Figure 11** Personal best proportional and integral gain ( $K_{PBPS}$  and  $K_{PBIS}$ ) with EU driving cycle, (a) after 1st iteration (b) after 2nd iteration (c) after 10th iteration (d) after 20th iteration

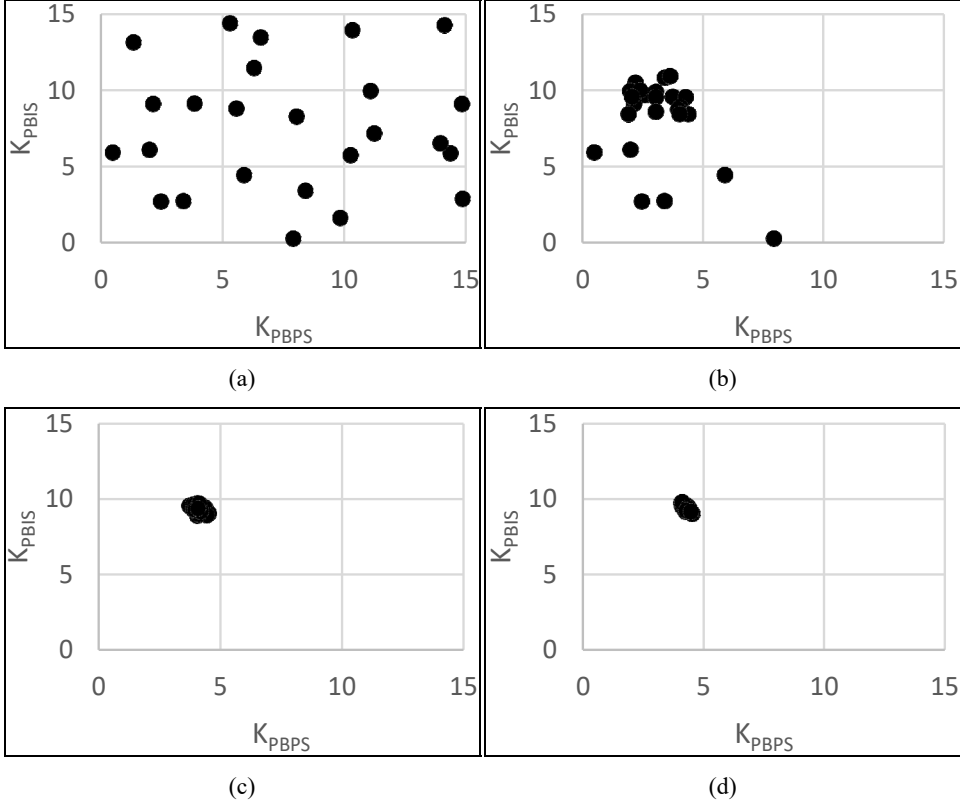


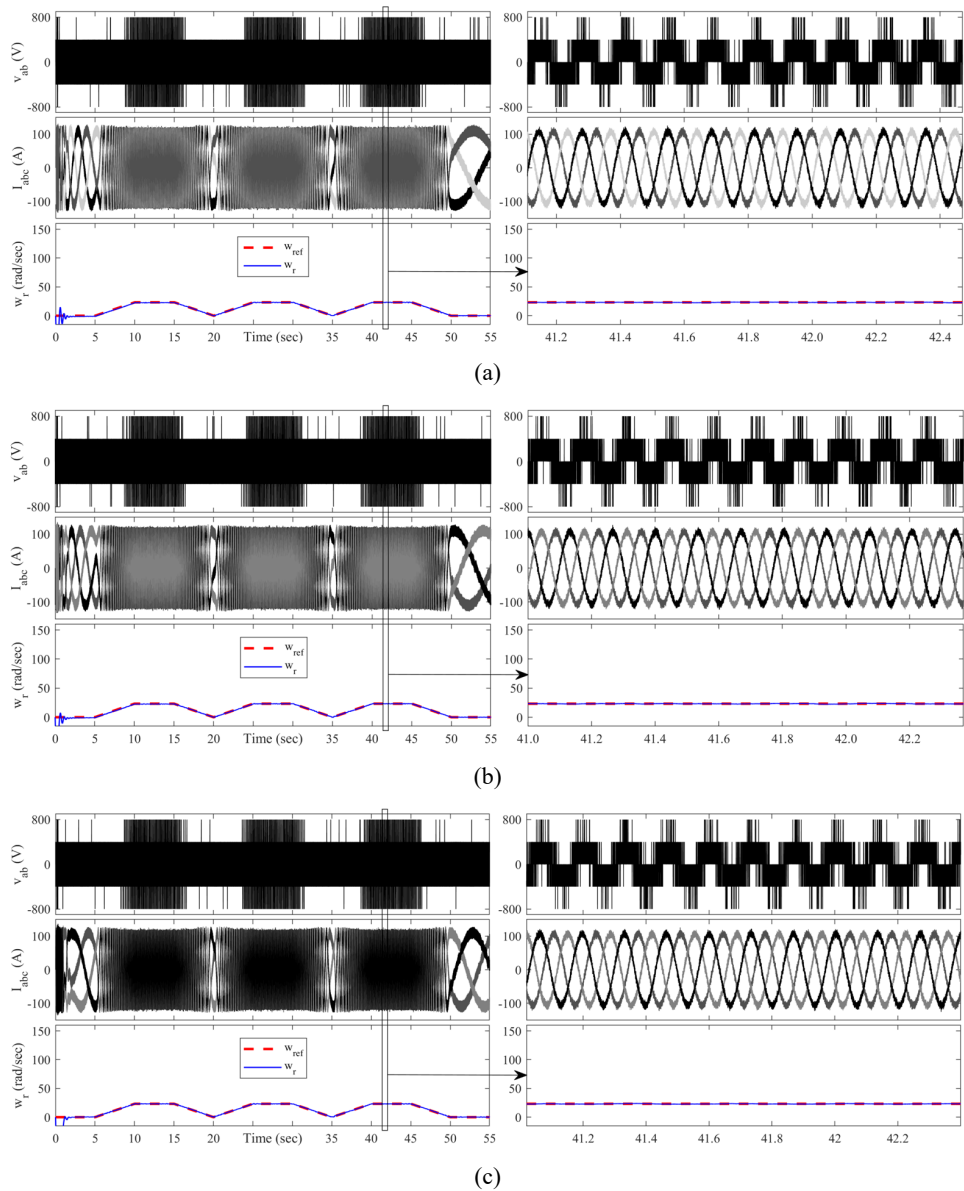
**Table 3** Global best values with different driving cycles

Driving cycle	$e_{\omega}$	$e_T$	$f_{GB}$	$K_{GBPS}$	$K_{GBIS}$
CBD	2.79989	43.78713	23.29351	7.821584	0.691534
COMMUTER	4.57442	44.83415	24.70428	5.782789	0.715844
EU	3.49922	40.14922	21.82422	4.328747	9.416067

### 3.2 Simulation results with different driving cycles

The performance of CHB3LI fed IMD is tested with CBD, COMMUTER, and EU driving cycle using MATLAB Simulink (Jain, 2017) and shown in Figures 12, 13, and 14.

**Figure 12** Performance of CHB3LI fed IMD with CBD driving cycle on different load, (a) 80% load (b) 90% load (c) 100% load (see online version for colours)



Each driving cycle performance is obtained on three different loading as listed in Table 2. The performance of IMD with each driving cycle on 80, 90, and 100% load is analysed in term of line voltage ( $V_{ab}$ ), 3-phase current ( $I_{abc}$ ), and rotor speed ( $\omega_r$ ). The performance of IMD with CBD driving cycle, along with zoomed view at steady-state, is shown in Figure 12. The IMD successfully runs with CBD driving cycle on 80, 90, and 100% loading. The three-phase current is stable while frequency is proportional to speed during the complete drive cycle. Average speed and torque errors during different modes of

CBD driving cycle are listed in Tables 4 and 7, respectively. The average speed and torque errors of various modes of CBD driving cycle are almost equal on all loadings except 100% loading. This proves the effectiveness of the PI speed controller with obtained optimum gain values.

**Figure 13** Performance of CHB3LI fed IMD with COMMUTER driving cycle, (a) 80% load (b) 90% load (c) 100% load (see online version for colours)

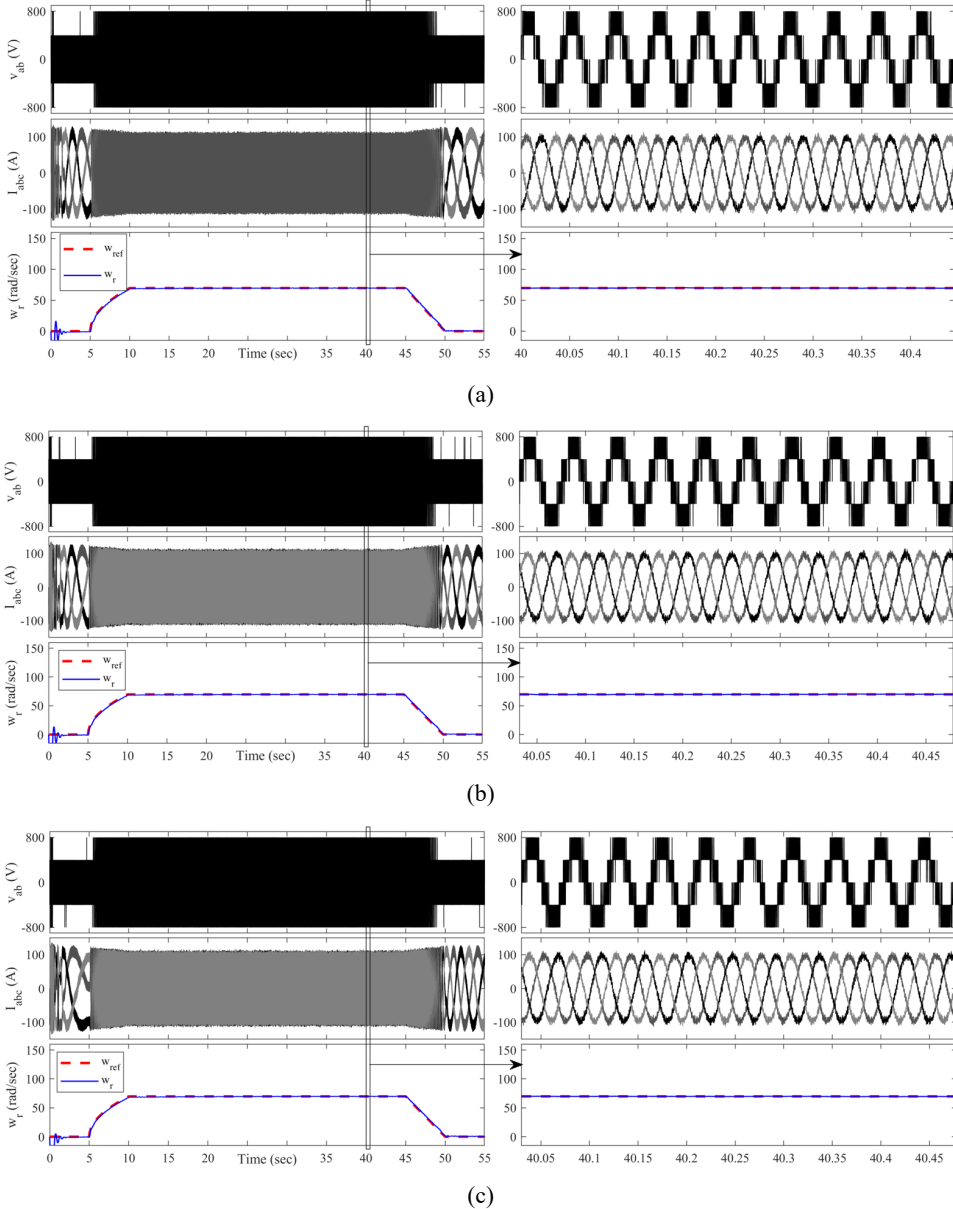
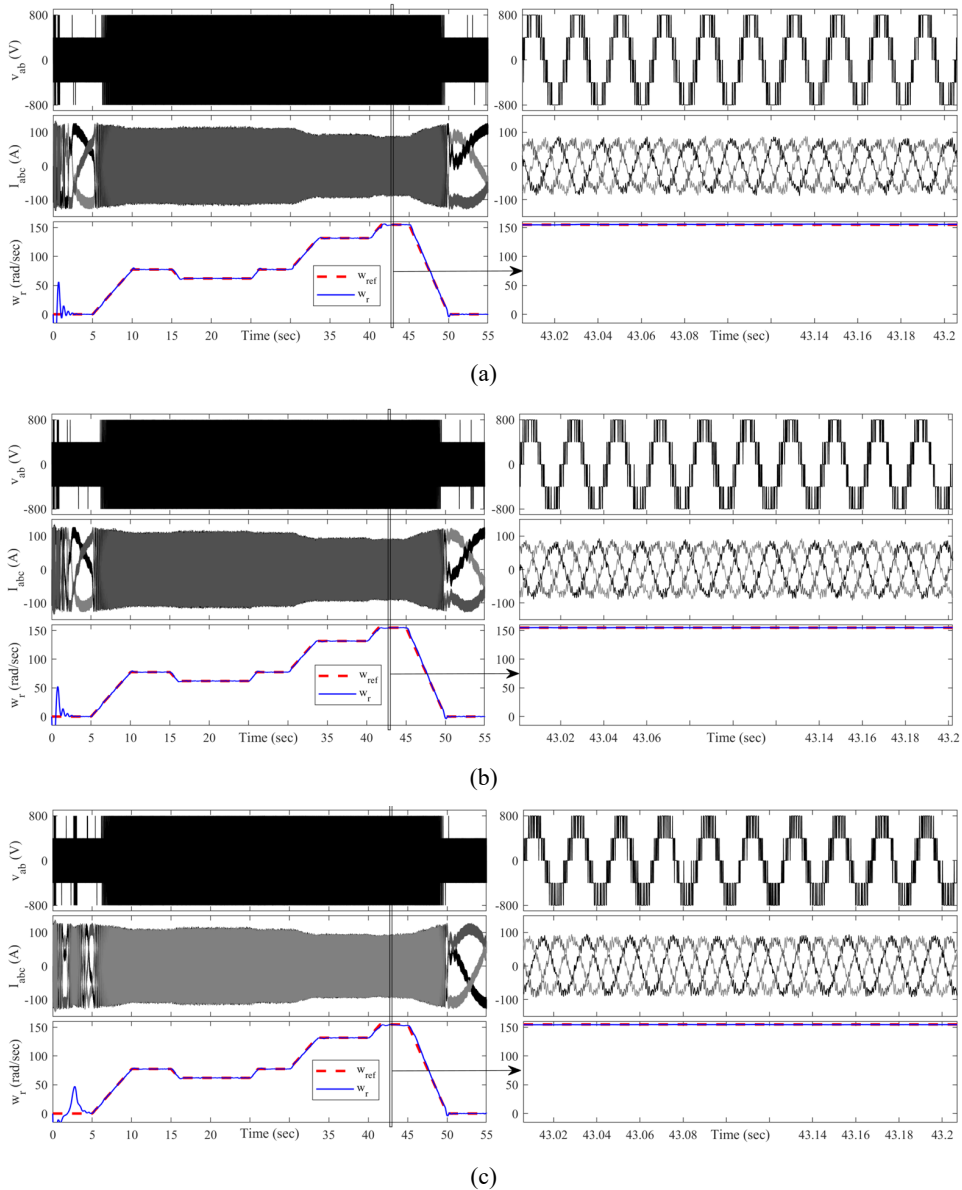


**Figure 14** Performance of CHB3LI fed IMD with EU driving cycle, (a) 80% load (b) 90% load (c) 100% load (see online version for colours)



The performance of CHB3LI fed IMD with COMMUTER driving cycle, along with zoomed view at steady-state, is given in Figure 13. The IMD successfully run with COMMUTER driving cycle on 80, 90, and 100% torque loading. The three-phase current amplitude is stable while frequency is proportional to speed during the complete duration of COMMUTER driving cycle. Average speed and torque error during different mode of COMMUTER driving cycle are listed in Tables 5 and 8, respectively. The average speed and torque error of each mode of COMMUTER driving cycle are almost equal on all

loading. This proves the effectiveness of the PI speed controller with obtained optimum gain values for COMMUTER driving cycle.

**Table 4** Average speed error during different mode and loading of CBD driving cycle

Average speed error	Percentage loading				
	80	85	90	95	100
$e_w(\delta_0)$	6.0740	6.3991	6.7095	7.2694	10.3357
$e_w(\delta_1)$	1.0256	1.0082	0.9490	0.7947	0.2658
$e_w(\delta_2)$	0.6034	0.6124	0.5838	0.5022	0.2283
$e_w(\delta_3)$	0.2049	0.2372	0.2633	0.2234	0.3657
$e_w(\delta_4)$	0.1774	0.1357	0.1476	0.1716	0.1906

**Table 5** Average speed error during different mode and loading of COMMUTER driving cycle

Average speed error	Percentage loading				
	80	85	90	95	100
$e_w(\delta_0)$	6.8424	7.2778	7.6839	8.0356	8.4063
$e_w(\delta_1)$	1.7052	1.7574	1.7636	1.7803	1.7299
$e_w(\delta_2)$	0.3292	0.3497	0.3734	0.3960	0.4032
$e_w(\delta_3)$	1.2457	1.2840	1.3585	1.4268	1.5080
$e_w(\delta_4)$	0.4241	0.4906	0.5737	0.6799	0.7794

**Table 6** Average speed error during different mode and loading of EU driving cycle

Average speed error	Percentage loading				
	80	85	90	95	100
$e_w(\delta_0)$	9.4510	10.1150	10.7598	11.9579	17.7903
$e_w(\delta_1)$	0.6245	0.5954	0.6086	0.6382	0.6445
$e_w(\delta_2)$	0.3094	0.3006	0.3110	0.3044	0.2945
$e_w(\delta_3)$	1.1059	1.1216	1.1055	1.0707	1.0943
$e_w(\delta_5)$	0.2697	0.2387	0.2644	0.2350	0.2386
$e_w(\delta_6)$	1.0869	1.1282	1.2457	1.1593	1.1574
$e_w(\delta_7)$	0.3344	0.3244	0.3297	0.3707	0.3221
$e_w(\delta_8)$	1.1334	1.1907	1.2670	1.3646	1.5078
$e_w(\delta_9)$	0.3273	0.3176	0.2748	0.3143	0.2608
$e_w(\delta_{10})$	1.8713	1.8683	1.9726	2.2078	2.4827
$e_w(\delta_{11})$	0.3911	0.3477	0.3927	0.3775	1.5575
$e_w(\delta_{12})$	2.1663	2.3000	2.4906	2.7186	3.7243
$e_w(\delta_4)$	0.3667	0.4152	0.3709	0.3775	0.4413

The performance of CHB3LI fed IMD with EU driving cycle, along with zoomed view at steady-state, is given in Figure 14. The IMD successfully run with EU driving cycle on 80, 90, and 100% torque loading. The three-phase current amplitude is stable while frequency is proportional to speed during the complete duration of EU driving cycle. Average speed and torque error during different mode of EU driving cycle are listed in

Tables 6 and 9, respectively. The average speed error of each mode of EU driving cycle are almost equal on all loading except 100% loading for  $\delta_0$ ,  $\delta_{11}$ , and  $\delta_{12}$ . The average torque errors of each mode of EU driving cycle are almost equal on all loading except 100% loading for  $\delta_0$ . This proves the effectiveness of the PI speed controller with obtained optimum gain values for EU driving cycle.

**Table 7** Average torque error during different mode and loading of CBD driving cycle

Average torque error	Percentage loading				
	80	85	90	95	100
$e_T(\delta_0)$	50.0839	50.1362	48.8891	47.4142	44.5990
$e_T(\delta_1)$	43.4146	43.3924	42.9760	42.9923	42.9245
$e_T(\delta_2)$	46.6924	46.5350	46.1432	45.8362	46.0407
$e_T(\delta_3)$	43.2220	43.2154	42.9745	42.6604	42.5134
$e_T(\delta_4)$	44.8812	44.5056	44.3512	44.2762	44.3862

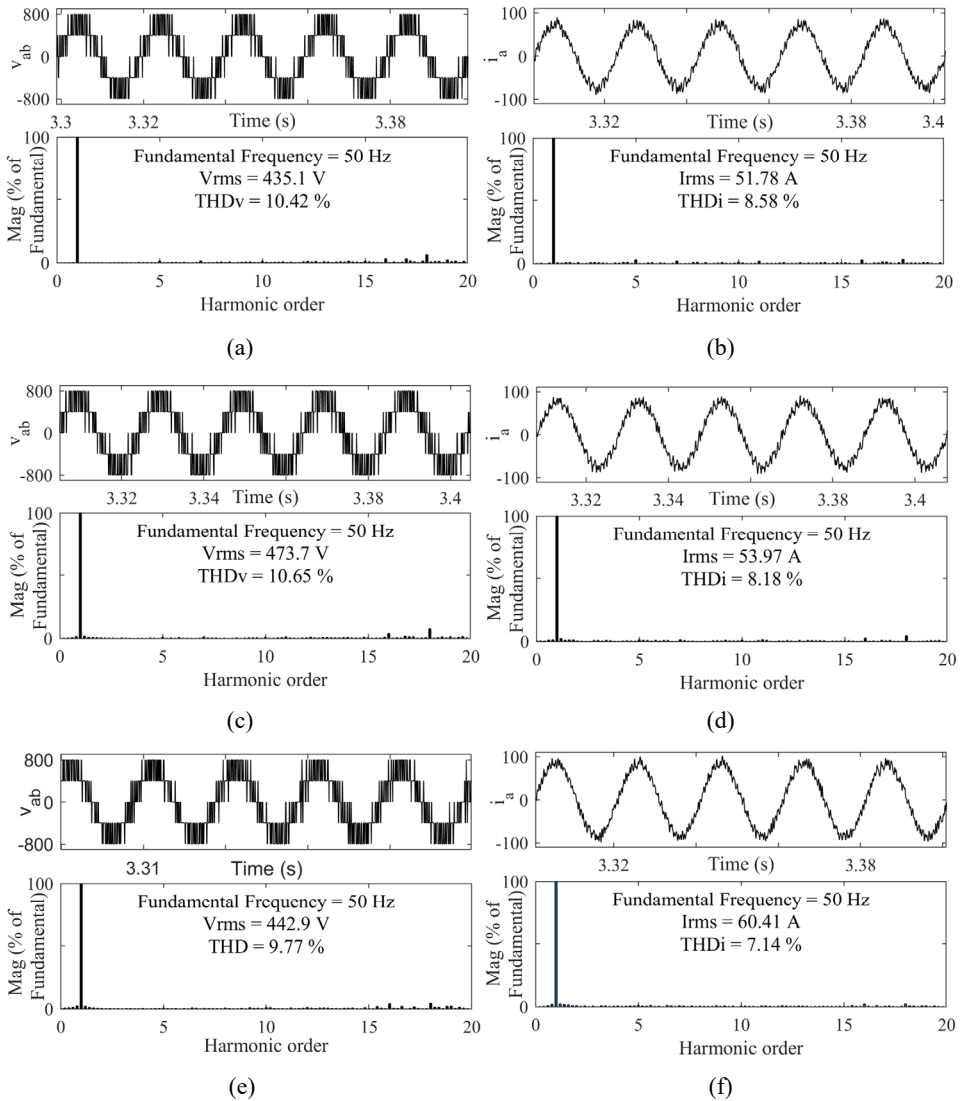
**Table 8** Average torque error during different mode and loading of COMMUTER driving cycle.

Average torque error	Percentage loading				
	80	85	90	95	100
$e_T(\delta_0)$	51.2086	51.4617	51.8318	51.5198	50.8078
$e_T(\delta_1)$	46.8062	46.4495	46.4084	45.7238	45.4457
$e_T(\delta_2)$	45.3044	44.7041	44.1913	43.1748	42.4559
$e_T(\delta_3)$	45.2237	45.2173	44.9712	44.7429	43.9725
$e_T(\delta_4)$	44.4184	44.4963	43.9005	43.8204	43.7362

**Table 9** Average torque error during different mode and loading of EU driving cycle

Average torque error	Percentage loading				
	80	85	90	95	100
$e_T(\delta_0)$	56.2599	55.5011	54.7073	51.2256	39.3300
$e_T(\delta_1)$	46.8578	46.4010	46.0889	45.6941	45.1403
$e_T(\delta_2)$	46.4767	45.4292	44.2196	43.4488	42.5642
$e_T(\delta_3)$	44.1595	43.2510	42.4576	41.7172	41.5269
$e_T(\delta_5)$	43.3316	43.0958	42.7484	42.1831	41.5059
$e_T(\delta_6)$	46.3972	45.8155	45.1565	44.2928	43.3804
$e_T(\delta_7)$	46.6351	45.3047	44.3904	43.1765	42.6061
$e_T(\delta_8)$	38.8612	39.3619	39.4101	40.2493	41.4088
$e_T(\delta_9)$	30.1318	28.8987	29.7254	31.1709	32.1857
$e_T(\delta_{10})$	28.1141	28.4064	28.7602	30.2278	31.4572
$e_T(\delta_{11})$	24.6433	25.9800	26.8442	28.0639	25.7239
$e_T(\delta_{12})$	39.8795	39.9052	39.6792	39.5506	38.0886
$e_T(\delta_4)$	45.0623	44.7806	44.6515	44.5141	44.1747

**Figure 15** THDv and THDi analysis of CHB-3LI fed IMD on various load at rated speed, (a) THDv on 80% load (b) THDi on 80% load (c) THDv on 90% load (d) THDi on 90% load (e) THDv on 100% load (f) THDi on 100% load

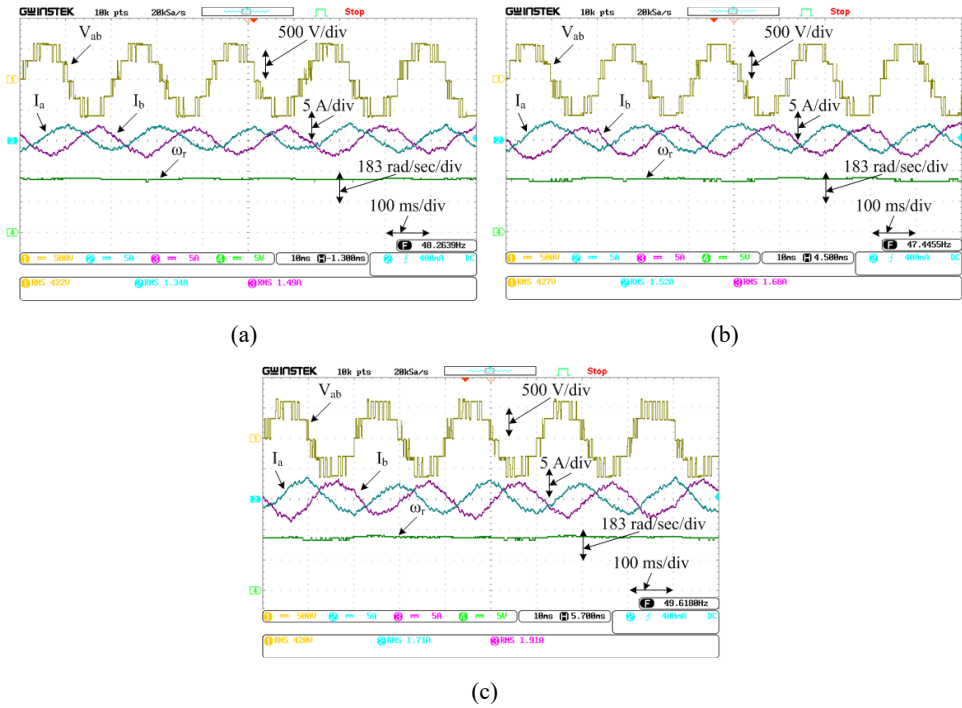


The power quality of CHB3LI is analysed in terms of THDv and THDi in voltage and current supplied to IM. The THDv and THDi is observed at 80, 90, and 100% load as shown in Figure 15. From Figure 15(a), 15(c) and 15(e), the observed THDv is between 9.77 to 10.65%, while, the observed voltage is between 435.1 to 473.7 V. From Figures 15(b), 15(d), and 15(f), the observed THDi is between 7.14 to 8.58%, while, the observed current is between 51.78 to 60.41 A. The change in loading from 80 to 100% is represented by increases in current from 51.78 to 60.41 A.



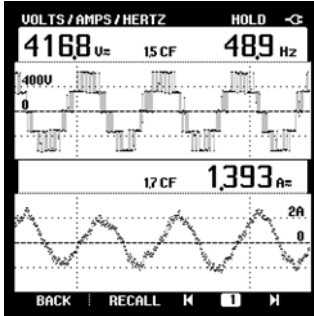
current, and rotor speed is sensed through TESTEC differential voltage probe, Tektronix A622 AC/DC current probe, FLUKE 80i-110s AC/DC current probe, and tacho-generator connected on motor shaft. The tacho-generator voltage is reduced further through potential divider circuit for feeding to dSPACE and recording on DSO. The results are obtained from the experimental setup under steady-state condition at 80, 90, and 100% load, as shown in Figure 17. From the shown experimental waveforms, it is observed that CHB3LI fed IMD maintains a constant speed and sinusoidal current waveform at 80, 90, and 100% load.

**Figure 17** Experimental performance of CHB3LI fed IMD during steady-state on different loads, (a) 80% load (b) 90% load (c) 100% load (see online version for colours)

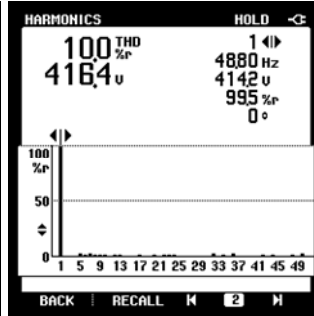


FLUKE 43B power quality analyser is used to observe the THDv and THDi at the output of CHB3LI. The experimental performance of CHB3LI in terms of THDv and THDi, is presented in Figure 18, at 80, 90, and 100% loads. The line-voltage and THDv is maintained constant between 412.9–416.4 V and 9.6–10.0%, at 80, 90, and 100% loads. The phase-current is 1.4, 1.57, and 1.721 A at 80, 90, and 100% load, respectively, while, THDi is maintained constant between 6.2–7.5%. This validates the presented concepts of controller optimisation for effective speed control with reduced THD of voltage and current supplied to the IM from the CHB3LI topology.

**Figure 18** Experimental performance of CHB3LI in terms of THDv and THDi with 80% load [Figures 18(a), 18(b) and 18(c)], 90% load [Figures 18(d), 18(e) and 18(f)], and 100% load [Figure 18(g), 18(h) and 18(i)], (a) line-voltage and phase current (b) harmonic spectrum of line-voltage (c) harmonic spectrum of phase current (d) line-voltage and phase current (e) harmonic spectrum of line-voltage (f) harmonic spectrum of phase current (g) line-voltage and phase current (h) harmonic spectrum of line-voltage (i) harmonic spectrum of phase current



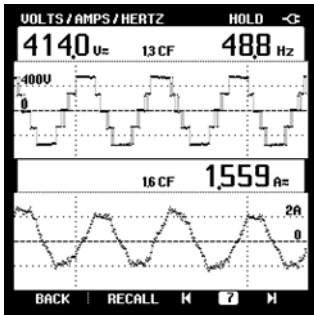
(a)



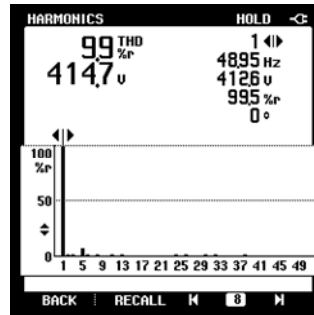
(b)



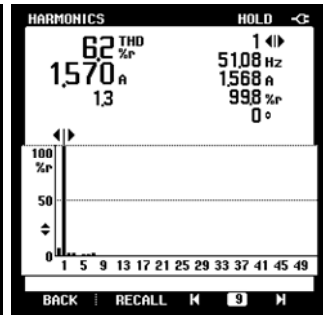
(c)



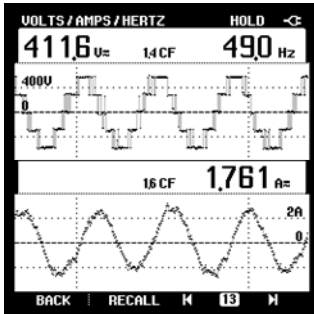
(d)



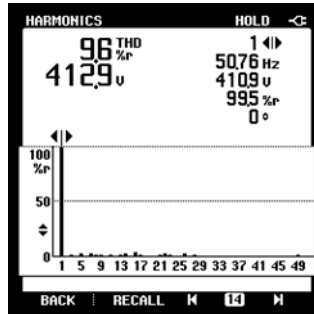
(e)



(f)



(g)



(h)



(i)

## 4 Conclusions

An IM has been operated successfully through CHB3LI topology for EV application. The complete IMD has been controlled through ICVC scheme with optimised speed controller. The optimised speed controller coefficients have been obtained using PSO technique for different driving cycles of the EV. The drive cycles used for this work are CBD, COMMUTER, and EU. The performance of CHB3LI fed IMD is successfully simulated with these driving cycles on different loadings based on the seating capacity of the EV. The simulated performance has demonstrated effective tracking of the speed in each drive cycle along with improved THD of voltage and current. The steady-state performance of CHB3LI fed IMD with optimised controller coefficients has been validated experimentally on a reduced rating laboratory setup. The presented results validate the proposed control and optimisation concepts and it is expected that these concepts shall be applicable to any driving cycle for EVs.

## References

- Armi, F., Manai, L. and Besbes, M. (2020) ‘Cascaded H-bridge inverter with reduced device count control considering harmonic distortion minimisation’, *Int. J. Power Electronics*, Vol. 11, No. 2, pp.139–159.
- Bansal, J.C. et al. (2011) *Inertia Weight Strategies in Particle Swarm Optimization*, IEEE, Salamanca, Spain.
- Hannana, M.A., Ali, J.A., Mohamed, A. and Hussain, A. (2018) ‘Optimization techniques to enhance the performance of induction motor drives a review’, *Renewable and Sustainable Energy Reviews*, Vol. 81, Part 2, pp.1611–1626.
- Jain, S. (2017) *Modeling and Simulation using MATLAB-Simulink*, Wiley, New Delhi.
- Jamwal, P.S. and Singh, S. (2016) ‘Speed controller optimization for PMSM drive using PSO algorithm’, in Pant, M. et al. (Eds.): *Proceedings of Fifth International Conference on Soft Computing for Problem Solving*, Springer, Singapore, pp.989–999.
- Jamwal, P.S., Singh, S. and Jain, S. (2022) ‘Indirect current vector controlled three-level inverter for induction motor driven electric vehicle’, in Kumar, S., Singh, B. and Singh, A.K. (Eds.): *Recent Advances in Power Electronics and Drives, Lecture Notes in Electrical Engineering*, Springer, Singapore, pp.575–585.
- Kennedy, J. and Eberhart, R. (1995) *Particle Swarm Optimization*, IEEE, Perth, WA, Australia.
- Kousalya, V., Rai, R. and Singh, B. (2022) ‘Sliding model-based predictive torque control of induction motor for electric vehicle’, *IEEE Transactions on Industry Applications*, Vol. 58, No. 1, pp.742–752.
- Krishnan, R. (2015) *Electric Motor Drives Modeling, Analysis, and Control*, Pearson, India.
- Kundu, S. et al. (2020) ‘Selective harmonics elimination for three-phase seven-level CHB inverter using backtracking search algorithm’, *Int. J. Power Electronics*, Vol. 11, No. 1, pp.1–19.
- Lammouchi, Z. and Barra, K. (2020) ‘Particle swarm weighting factor optimisation for predictive control of three level inverter with balanced voltages’, *International Journal of Power Electronics*, Vol. 12, No. 3, pp.302–316.
- Mahindra Electric e2o Plus (n.d.) [online] <https://www.mahindraelectric.com/pdfs/e2oPlus-Brochure.pdf> (accessed 25 October 2020).
- Mishra, P. and Maheshwari, R. (2020) ‘Design analysis and impacts of sinusoidal LC filter on pulse width modulated inverter fed induction motor drive’, *IEEE Transactions on Industrial Electronics*, Vol. 67, No. 4, pp.2678–2688.

- Nagadurga, T., Narasimham, P.V.R.L. and Vakula, V.S. (2021) 'Harness of maximum solar energy from solar PV strings using particle swarm optimisation technique', *International Journal of Ambient Energy*, Vol. 42, No. 13, pp.1506–1515.
- Poorfakhraei, A., Narimani, M. and Emadi, A. (2021) 'A review of multilevel inverter topologies in electric vehicles current status and future trends', *IEEE Open Journal of Power Electronics*, Vol. 2, No. 1, pp.155–170.
- Prabhakar, K.K., Chinthakunta, U.R., Singh, A.K. and Kumar, P. (2018) 'Efficiency and performance analysis of DTC-based IM drivetrain using variable dc-link voltage for electric vehicle applications', *IET Electrical Systems in Transportation*, Vol. 8, No. 3, pp.205–214.
- Rohit, C., Darji, P. and Jariwala, H. (2022) 'Modelling and control of static synchronous series compensator interfaced with DFIG based wind farm using PSO for SSR alleviation', *International Journal of Ambient Energy*, Vol. 43, No. 1, pp.6449–6462.
- Singh, S. and Singh, B. (2014) 'Optimized passive filter design using modified PSO algorithm for 12 pulse converter fed LCI SM drive', *IEEE Transactions on Industry Applications*, Vol. 50, No. 4, pp.2681–2689.
- Suresh, M. et al. (2020) 'An enhanced multiobjective particle swarm optimisation algorithm for optimum utilisation of hybrid renewable energy systems', *International Journal of Ambient Energy*, pp.1–9.
- Xu, B., Shi, J., Li, S. and Li, H. (2022) 'A study of vehicle driving condition recognition using supervised learning methods', *IEEE Transactions on Transportation Electrification*, Vol. 8, No. 2, pp.1665–1673.

## Appendix A

### Parameters for simulation

- *Parameters of IM:* Rated power ( $P_{\text{rat}}$ ) = 37 kW, rated speed ( $\omega_{\text{rat}}$ ) = 155 rad/sec, RMS line voltage ( $V_L$ ) = 400 V, rated frequency ( $f_{\text{rat}}$ ) = 50 Hz, stator resistance ( $R_S$ ) = 0.08233  $\Omega$ , stator inductance ( $L_S$ ) = 0.000724 H, rotor resistance ( $R_R$ ) = 0.0503  $\Omega$ , rotor inductance ( $L_R$ ) = 0.000724 H, mutual inductance ( $L_M$ ) = 0.02711 H, inertia ( $J$ ) = 0.37 kg.m<sup>2</sup>, friction factor ( $F$ )  $p$  = 0.02791 Nms, number of poles ( $P$ ) = 4, rated torque ( $T_{\text{rat}}$ ) = 238.73 Nm, and sampling time ( $T_S$ ) = 50  $\mu$ s.
- *Parameters of inverter:* dc link voltage ( $V_{\text{dc}}$ ) = 400 V, switching frequency ( $f_{\text{sw}}$ ) = 1 kHz.
- *Parameters of driving cycle:* Size of section ( $s_{\text{dc}}$ ) = 5, number of section ( $n_{\text{dc}}$ ) = 11.
- *Parameters of PSO technique:* Number of particles ( $N_P$ ) = 25, number of iteration ( $N_i$ ) = 20, minimum value of proportional gain ( $K_{\text{PSmin}}$ ) = 0, maximum value of proportional gain ( $K_{\text{PSmax}}$ ) = 15, minimum value of integral gain ( $K_{\text{ISmin}}$ ) = 0, maximum value of integral gain ( $K_{\text{ISmax}}$ ) = 15, speed fitness weightage ( $w_{\omega f}$ ) = 0.5, torque fitness weightage ( $w_{Tf}$ ) = 0.5, and inertia weight ( $w_i$ ) = 0.7298.

**Appendix B***Parameters for experimental setup*

- *Parameters of IM:* Rated power ( $P_{\text{rat}}$ ) = 750 W, rated speed ( $\omega_{\text{rat}}$ ) = 147.65 rad/sec, RMS line voltage ( $V_L$ ) = 415 V, rated frequency ( $f_{\text{rat}}$ ) = 50 Hz, stator resistance ( $R_S$ ) = 9.795  $\Omega$ , stator inductance ( $L_S$ ) = 0.0698 H, rotor resistance ( $R_R$ ) = 9.975  $\Omega$ , rotor inductance ( $L_R$ ) = 0.0349 H, mutual inductance ( $L_M$ ) = 0.6496 H, inertia ( $J$ ) = 0.012 kg.m<sup>2</sup>, friction factor ( $F$ ) = 0.002241 Nms, number of poles ( $P$ ) = 4, rotor flux linkage ( $\lambda_r$ ) = 0.97 Wb, rated torque ( $T_{\text{rat}}$ ) = 5.08 Nm, and sampling time ( $T_s$ ) = 150  $\mu$ s.